Chinese Journal of Chemical Engineering 48 (2022) 227–235

Contents lists available at ScienceDirect

Chinese Journal of Chemical Engineering

journal homepage: www.elsevier.com/locate/CJChE

Full Length Article

Chiral LVFFARK enantioselectively inhibits amyloid-β protein fibrillogenesis

Wei Liu [#], Xueting Sun [#], Xiaoyan Dong, Yan Sun [*]

Department of Biochemical Engineering, School of Chemical Engineering and Technology and Key Laboratory of Systems Bioengineering and Frontiers Science Center for Synthetic Biology (Ministry of Education), Tianjin University, Tianjin 300350, China

ARTICLE INFO

Article history:
Received 12 April 2021
Received in revised form 19 May 2021
Accepted 21 May 2021
Available online 20 July 2021

Keywords:
Alzheimer's disease
Amyloid-β protein
Protein aggregation
Chirality
Inhibitor
Heptapeptide

ABSTRACT

The modulation of protein aggregation is involved not only in biochemical engineering processes, but also in *in vivo* biological events such as Alzheimer's disease (AD) that features amyloid-β protein (Aβ) deposits. Inspired by the different pharmacological efficacy of enantiomers, taking heptapeptide LVFFARK (LK7) as an example, herein the chiral influence of peptide inhibitors on Aβ fibrillogenesis and cytotoxicity was investigated by extensive biophysical and biological analyses. It was intriguing to find that although both L-LK7 and D-LK7 could inhibit Aβ aggregation in a concentration-dependent manner, it was the D-enantiomer that exhibited chirality preference and selectivity for modulation of Aβ self-assembly. As compared with L-LK7 at the same conditions, D-LK7 showed significantly enhanced potency on suppressing cross-β sheet formation, fibrillar Aβ aggregates deposition, Aβ conformational transition, and Aβ-triggered neurotoxicity on cultured cells. For instance, L-LK7 and D-LK7 rescued cells by increasing cell viability from 60% to 62% and 84% at 100 $\mu mol \cdot L^{-1}$, respectively. The chiral discrimination of L-LK7 and D-LK7 was further validated by the different elimination efficiency on amyloid accumulation in AD model nematodes. It is considered that the higher binding affinity of D-LK7 to Aβ monomers than that of L-LK7 resulted in the stronger inhibition effect. This work provided new insights into understanding chirality in the interaction with Aβ and the consequent inhibitory effect, and would contribute to the design of anti-amyloid agents.

1. Introduction

Proteins are the basic building blocks of life and the most common products in biopharmaceutical field. However, the unstable and transient nature of proteins makes them vulnerable to aggregation, causing the loss of bioactivity and functionality [1,2]. Thus, modulation of protein aggregation is one key issue in biochemical engineering as well as in life science. Amyloid-β protein (Aβ), the hydrophobic peptide that consists of 39–42 amino acid residues, can spontaneously assemble into toxic oligomers, protofibrils and insoluble fibrillar aggregates containing β-sheet-rich structures [3–5]. Recent researches have revealed that the deposition of Aβ species in cerebrum is pathologically related to Alzheimer's disease (AD), which has afflicted about 50 million people around the world and costed more than 1 trillion USD [6]. According to the "amyloid cascade hypothesis", amyloid oligomerization and aggregation plays a central role in the progress of AD, resulting in oxidative stress, neuroinflammation, neurons death and ultimately neurons dysfunction [7–9]. The soluble Aβ oligomers that form during the self-aggregation of Aβ monomers have been considered as the most neurotoxic ones. These Aβ species can interact with neurons, leading to the disintegration of neuronal membranes and neurodegeneration. Therefore, design of Aβ modulators that can affect the on-pathway amyloid aggregation and reduce Aβ-induced cytotoxicity has emerged as a promising therapeutic strategy for AD.

Currently, there are various Aβ modulators, such as peptides, proteins, antibodies, small molecules, polymers and functional nanoparticles [10–15]. These modulators can interact with Aβ species via hydrophobic and electrostatic interactions, modulating Aβ aggregation, preventing the formation of toxic oligomers, and then rescuing neurons from Aβ species-induced cytotoxicity. Of those, peptide-based or peptide-derived inhibitors have attracted increased attention because of the favorable biocompatibility, facile modification, better blood–brain barrier (BBB) penetration, superior specificity and selectivity, and highly developed methods of rational design [10,16]. Based on their relevance to Aβ sequence, peptide

* Corresponding author.
E-mail address: ysun@tju.edu.cn (Y. Sun).
[#] Authors contributed equally to this work.

https://doi.org/10.1016/j.cjche.2021.05.033
1004-9541/

inhibitors can be cataloged into two types including those derived from Aβ fragments such as central hydrophobic core (CHC) and C-terminal domains, and those not derived from Aβ fragments [17–20]. Since Aβ aggregation is a cascade process of self-assembly with the CHC as a "nucleation site", the CHC-derivatives that homologous to the self-recognition fragment can perturb the self-association of Aβ monomers to modulate Aβ aggregation. On the basis of this concept, a heptapeptide LVFFARK (LK7), was designed and has been demonstrated to be an Aβ modulator [21–23]. It is proposed that LK7 would interact with the corresponding region of Aβ via KLVFF, and the binding could be further enhanced by the electrostatic interactions of positively charged residues, RK in LK7, with the negatively charged ED in Aβ. Nevertheless, the defects of LK7, such as moderate-to-poor inhibition effect, high propensity to self-assembly and the resulting toxic aggregates limited its clinical application, which prompted us to further improve its performance.

For pharmaceutical candidates, chirality is an extremely important principle that needs to be considered because chirality could decide the biological functions of many drug molecules. Usually, just one enantiomer is pharmaceutically active, whereas the other is inactive or exerts severe adverse effects [24,25]. Such as the widely used penicillamine, the D-enantiomer is pharmacological effective, while the L-enantiomer is considerable toxicity [26]. As for Aβ aggregation and inhibition, Chirality also plays a critical role due to the specific orientation of Aβ species that consists of L-amino acids. It has been demonstrated that Aβ aggregation is sensitive to a chiral environment and the chiral modulators can enantioselectively inhibit Aβ aggregation [27–31]. From peptides to nanoparticles, most of chiral modulators exhibit varied biological activities towards Aβ [30,31]. These chiral modulators may provide different conformations to match Aβ species, leading to distinct recognition and amyloid aggregation behaviors. Thus, the chiral recognition between Aβ and modulators would provide a new perspective for the design of more potent Aβ modulators.

In this work, to improve the inhibitory potency of L-LK7 as well as to reveal the chiral discrimination of two enantiomers, the effect of L-LK7 and D-LK7 on modulating Aβ fibrillogenesis was investigated and compared by thioflavin T (ThT) fluorescence assay, atomic force microscopy (AFM) imaging, circular dichroism (CD) spectroscopy, cell viability, and *C. elegans* experiments. The molecular mechanisms of enantiomers were further elucidated by molecular docking calculation. Results indicated the enantioselectivity of chiral LK7 on suppression of Aβ fibrillogenesis.

2. Materials and Methods

2.1. Materials

Synthetic $A\beta_{42}$ and $A\beta_{40}$ (>95% purity) were obtained from GL Biochem (Shanghai, China). Enantiomeric heptapeptide L-LK7 and D-LK7 (>95% purity) were purchased from ZiYu Biotechnology (Shanghai, China). 1,1,1,3,3,3-hexafluoro-2-propanol (HFIP), dimethyl sulfoxide (DMSO), thioflavin T (ThT), and 3-(4,5-dimethyl thiazol-2-yl)-2,5-diphenyltetrazolium bromide (MTT) were all purchased from Sigma-Aldrich (St. Louis, MO, USA). Human neuroblastoma SH-SY5Y cells were obtained from the Cell Bank of the Chinese Academy of Sciences (Shanghai, China). Dulbecco's modified Eagle's medium/Ham's F-12 (DMEM/F12) were received from Gibco Invitrogen (Grand Island, NY, USA). All other chemicals with analytical regent grade were purchased from local suppliers.

2.2. Aβ sample pretreatment and incubation

To obtain monomeric Aβ sample, before all aggregation assays, the commercial lyophilized Aβ powder should be treated with HFIP [32]. According to previous proposal, Aβ powder was firstly added to HFIP (1 $mg \cdot ml^{-1}$) and kept steady at 4 °C for 2 h. Then, the solution was sonicated for several minutes in an ice bath to destroy the pre-existing Aβ fibrils. Finally, the HFIP was removed via freeze-drying, and the lyophilized Aβ powder was stored at −20 °C immediately. Prior to use, Aβ was dissolved in 20 $mmol \cdot L^{-1}$ NaOH to 275 $\mu mol \cdot L^{-1}$, centrifuged at 16,000*g* for 20 min, and the 80% supernatant was diluted with 100 $mmol \cdot L^{-1}$ PBS buffer (100 $mmol \cdot L^{-1}$ PB + 10 $mmol \cdot L^{-1}$ NaCl, pH 7.4) to a concentration of 25 $\mu mol \cdot L^{-1}$. L-LK7/D-LK7 at different concentrations were added in the same time. The above prepared Aβ solution was incubated for 48 h at 37 °C, 150 $r \cdot min^{-1}$ in an incubator.

2.3. ThT fluorescence assays

For assessing cross-β sheet structures in Aβ species, ThT fluorescence experiments were conducted using a fluorescence spectrometer (PerkinElmer, LS-55, Waltham, MA). Briefly, a volume of 200 μl $A\beta_{42}$ sample was added into a quartz cell containing 2 ml of ThT (25 $\mu mol \cdot L^{-1}$ ThT in 100 $mmol \cdot L^{-1}$ PBS buffer) solution. The fluorescence intensity at 480 nm was measured with excitation wavelength at 440 nm. The fluorescence signal of buffer and peptide inhibitor was subtracted as a background. Final data were the average of three independent experiments and normalized with samples containing $A\beta_{42}$ alone.

For monitoring $A\beta_{40}$ aggregation kinetics, samples (200 μl in 100 $mmol \cdot L^{-1}$ PBS buffer) containing 25 $\mu mol \cdot L^{-1}$ $A\beta_{40}$ monomers, 25 $\mu mol \cdot L^{-1}$ ThT, and different concentrations of L-LK7/D-LK7 were added into a 96-well plate. The fluorescence signal was measured using a microplate reader (TECAN, Infinite M200 Pro, Salzburg, Austria) at 10 min reading intervals. The time-dependent fluorescence curves were fitted using the following Boltzmann model:

$$y = y_0 + \frac{y_{max} - y_0}{1 + \exp(-k(t - t_{1/2}))} \quad (1)$$

where y_0 and y_{max} are the minimum and maximum fluorescence values, respectively. y represents the fluorescence value at time t. k and $t_{1/2}$ are the elongation rate constant and the time when the fluorescence value reaches 50% of maximum fluorescence value. The lag time (T_{lag}) of $A\beta_{40}$ was calculated by the following equation:

$$T_{lag} = t_{1/2} - 2/k \quad (2)$$

2.4. Atomic force microscopy (AFM) imaging

The morphology of Aβ species and L-LK7/D-LK7 were observed by AFM (Benyuan, CSPM5500, Guangzhou, China) under air condition. Aβ samples without or with different concentrations of inhibitors were incubated at 37 °C for 72 h. For acquiring the morphology of Aβ species, 50 μl well-mixed sample was dropped on a freshly peeled mica flake and kept steady for 5 min. The mica was then washed with 8 ml ultrapure water to remove salts in PBS buffer and dried by N_2 stream. Images were taken at 1024 × 1024 pixel resolution under tapping mode.

2.5. Circular dichroism (CD) spectroscopy

After the protein aggregated, the conformational information of $A\beta_{42}$ was investigated using a CD spectrometer (JASCO, J-810, Japan). The ellipticity (190–260 nm) was recorded using a 1 mm path length quartz cell at 100 $nm \cdot min^{-1}$ scanning speed and 1 nm bandwidth. The contribution of L-LK7/D-LK7 and buffer to the CD signal was subtracted as background. The CD spectra of L-LK7/D-LK7 at 200 $\mu mol \cdot L^{-1}$ was obtained by subtracting the signal of buffer.

2.6. MTT cytotoxicity assay

Human SH-SY5Y cells were cultured in DMEM/F12 (10% FBS, 1% penicillin- streptomycin antibiotic) under 5% CO_2 humidified cell incubator at 37 °C. Cells at a density of 8×10^3 cells/well (80 μl) were seeded into a 96-well plate and cultured for 24 h. 20 μl of aged $A\beta_{42}$ (25 $\mu mol \cdot L^{-1}$) sample or inhibitor was introduced to each well and incubated for another 24 h. Followed by addition of 10 μl MTT solution (5.5 $mg \cdot ml^{-1}$ in PBS buffer) and incubation for 4 h, the culture medium was removed by centrifuge at 1500 $r \cdot min^{-1}$. Afterwards, a volume of 100 μl DMSO was added to dissolve formazan crystals in the precipitated cells. Finally, the absorbance at 570 nm was measured by a microplate reader. The cells treated with PBS buffer were set to 100% as control, and other groups were normalized with the control. The data were the average of six replicates and represented as mean ± SD. Statistical analyses were determined by one-way ANOVA with Tukey's multiple comparison test.

2.7. AD model experiments

The transgenic CL2006 nematodes were fed with *E. coli* OP50 on nematode growth medium (NGM) at 20 °C. For *in vivo* ThT staining of Aβ deposits, L4 larvae nematodes were cultured with L-LK7/D-LK7 on NGM plates for 3 days. The worms were fixed with 4% paraformaldehyde for 24 h, and stained with 25 $\mu mol \cdot L^{-1}$ ThT for 4 h. Then, the nematodes were mounted on a glass slide and observed by a fluorescence microscopy (Nikon, TE2000-U, Japan).

2.8. Molecular docking

The flexible ligand (L-LK7/D-LK7) was docked with receptor $A\beta_{40}$/$A\beta_{42}$ monomer (PDB entry: 2LFM/1IYT) using AutoDock Vina (http://vina.scripps.edu) [33–35]. The structures of chiral heptapeptides and $A\beta_{40}$/$A\beta_{42}$ monomer were prepared by AutoDock Tools in the standard manner. All torsion angles were considered flexible and other parameters were set as default. Docking models of LK7/Aβ complexes were captured using visual molecular dynamics (VMD) tools.

3. Results and Discussion

3.1. Inhibitory effect of enantiomers on Aβ fibrillization

ThT dye can bind to cross-β sheet structures exist in Aβ species and show enhanced fluorescence signal, so ThT fluorescence test was first performed to investigate the inhibitory effect of L-LK7 and D-LK7 on Aβ fibrillization. As shown in Fig. 1, enantiomers impeded $A\beta_{42}$ aggregation in a dose-dependent manner, and the inhibitory effect of D-LK7 was better than L-LK7 at the same concentrations. L-LK7 changed the final ThT fluorescence of $A\beta_{42}$ from 100% to 101%, 79%, 63% and 57% at molar ratios of 0.5:1, 1:1, 2:1 and 4:1 (inhibitor:$A\beta_{42}$, $A\beta_{42}$ = 25 $\mu mol \cdot L^{-1}$), respectively. By contrast, D-LK7 reduced ThT fluorescence intensity to 93%, 36%, 24% and 18% at the corresponding molar ratios.

Previous researches have indicated that chiral inhibitors could modulate Aβ aggregation in different manners [36–38], thus the aggregation kinetics of $A\beta_{40}$ with varying concentrations of L-LK7/D-LK7 were measured by *in situ* ThT fluorescence assay. $A\beta_{40}$ alone showed a typical sigmoidal growth curve with a lag phase, a fast growth phase and a plateau phase, which is consistent with literature [22]. Addition of L-LK7/D-LK7 to $A\beta_{40}$ led to a decrease of fluorescence intensity at plateau phase (Fig. 2). However, due to the lower hydrophobicity and aggregation propensity of $A\beta_{40}$, the ThT fluorescence intensities of $A\beta_{40}$ with enantiomeric heptapeptide at plateau phase were slightly lower than that of $A\beta_{42}$. To elucidate the difference of chiral inhibitors on $A\beta_{40}$ fibrillization, the aggregation kinetics curves of $A\beta_{40}$ were fitted by Eq. (1), and the lag time values were calculated by Eq. (2) and are listed in Table 1. As shown in Fig. 2 and Table 1, L-LK7 prolonged the lag times of $A\beta_{40}$ at lower concentrations (L-LK7:$A\beta_{40}$ = 0.5:1, 1:1, 2:1), but it shortened the lag time at higher concentration (L-LK7:$A\beta_{40}$ = 4:1). This phenomenon is similar to our previous work and it is considered that the self-assembly character of LK7 at high concentration may lead to form LK7 aggregates, resulting in the acceleration of Aβ aggregation [21,39]. By contrast, D-LK7 shortened the lag time of $A\beta_{40}$ at 12.5 and 25 $\mu mol \cdot L^{-1}$ (D-LK7:$A\beta_{40}$ = 0.5:1 and 1:1), and completely inhibited $A\beta_{40}$ fibrillization at 50 and 100 $\mu mol \cdot L^{-1}$ (D-LK7:$A\beta_{40}$ = 2:1 and 4:1). Thus, it can be concluded that D-LK7 facilitated $A\beta_{40}$ nucleation, which is consisted with the finding that D-RK10 accelerated Aβ fibrillization [36]. The aggregation kinetics assay indicates the effects of chiral heptapeptides on $A\beta_{40}$ nucleation were different from each other.

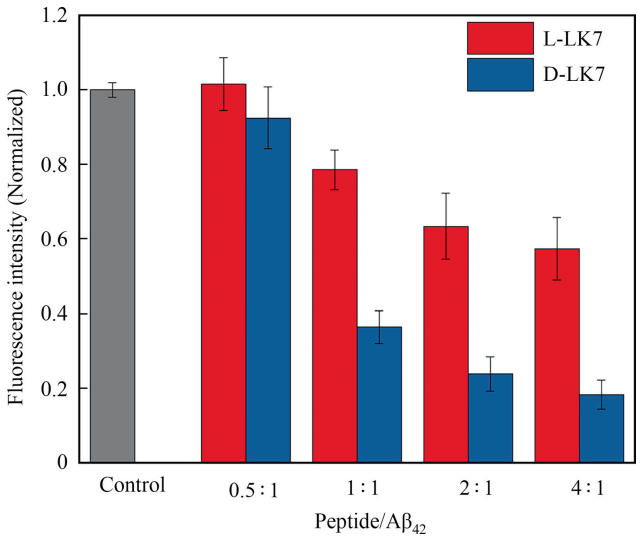

Fig. 1. ThT fluorescence intensity of $A\beta_{42}$ aggregated with enantiomeric inhibitors at different molar ratios for 48 h. The concentration of $A\beta_{42}$ was 25 $\mu mol \cdot L^{-1}$.

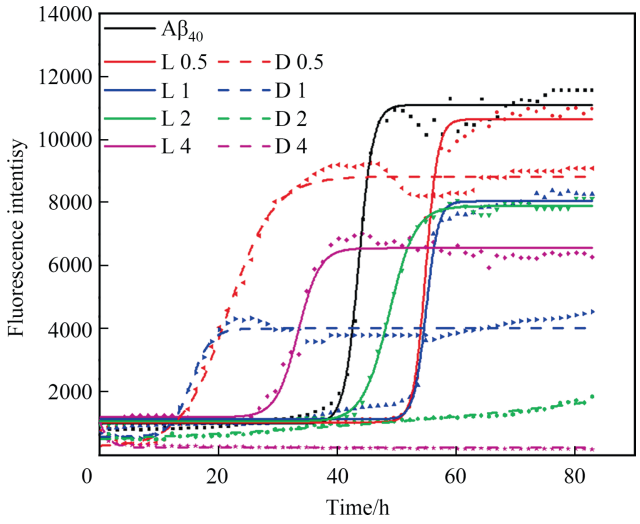

Fig. 2. Aggregation kinetics of $A\beta_{40}$ incubated with different concentrations of L-LK7/D-LK7. The curves were obtained by fitting with the Boltzmann function (Eq. (1)). L and D represent L- and D-enantiomer, respectively, and the following number represents the molar ratio of inhibitor to $A\beta_{40}$.

Table 1
Lag time values of $A\beta_{40}$ incubated with L-LK7/D-LK7 summarized from Fig. 2. The lag phase time of $A\beta_{40}$ is 45.2 h

L-LK7/$A\beta_{40}$	Lag time/h	D-LK7/$A\beta_{40}$	Lag time/h
0.5	56.8	0.5	22.1
1	56.9	1	16.6
2	49.6	2	ND
4	34.4	4	ND

3.2. Influence of enantiomers on the morphology of Aβ aggregates

To gain insight to the morphological changes of Aβ incubated without or with enantiomeric inhibitors, AFM image test was conducted. As illustrated in Fig. 3, two enantiomers exhibited high self-assembly performance after incubation for 72 h. L-LK7 aggregated into a twisted fibrillar species and D-LK7 formed amorphous aggregates and straight fibrils with a length of several micrometers. The difference in self-assembly ability of chiral heptapeptides may contribute to various inhibitory efficiency for blocking Aβ aggregation.

Then, the morphology of $A\beta_{40}$ aggregates was visualized in Fig. 4. $A\beta_{40}$ alone aggregated into dense and entangled fibrillar networks, similar to published reports [40,41]. Addition of L-LK7 led to the formation of less entangled, short and broken fibrils. Furthermore, the amount of $A\beta_{40}$ fibrils decreased significantly with increasing L-LK7 concentration. Remarkably, more obvious morphological changes were observed by incubating $A\beta_{40}$ with different concentration of D-LK7. At the molar ratios of D-LK7:$A\beta_{40}$ = 2:1, the fibrillar species transformed into amorphous structures; and at D-LK7:$A\beta_{40}$ = 4:1, the $A\beta_{40}$ aggregates completely disappeared. The morphology of $A\beta_{42}$ aggregates in the presence of enantiomeric inhibitors was also imaged and illustrated in Fig. 5, showing similar results. Above AFM imaging is in agreement with ThT fluorescence data, indicating the stronger inhibition of D-LK7 than L-LK7 on Aβ fibrillization.

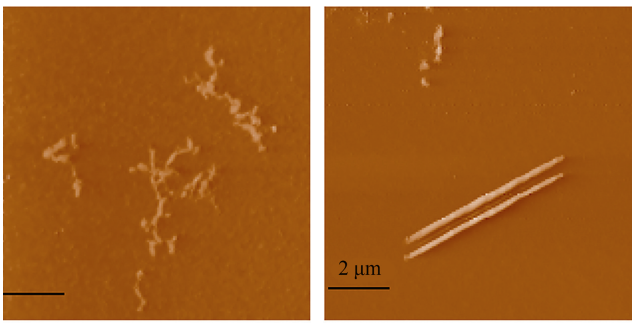

Fig. 3. Self-aggregation of L-LK7/D-LK7 obtained by incubation at 200 μmol·L^{-1} for 72 h.

3.3. Effect of enantiomers on the Aβ conformational transition

A series of conformational transition occurs during Aβ aggregation, which results in Aβ species with β-sheet-rich structures. Therefore, the ability of enantiomers on preventing Aβ conformational switch was assessed by CD spectroscopy. As expected, enantiomers showed similar but opposite CD signals, which indicates the mirror structures (Fig. 6(a)). At the initial state, $A\beta_{42}$ monomers adopted a random coil conformation with a negative peak at 199 nm (Fig. 6(b), black line). After 48 h incubation, $A\beta_{42}$ aggregates formed β-sheet structures, showing one negative valley at 216 nm and one positive peak at 197 nm. L-LK7 and D-LK7 decreased the negative ellipticity value at 216 nm, demonstrating the enantiomers could prevent conformational transition of $A\beta_{42}$ from native disordered coil to β-sheet structures. To further assess

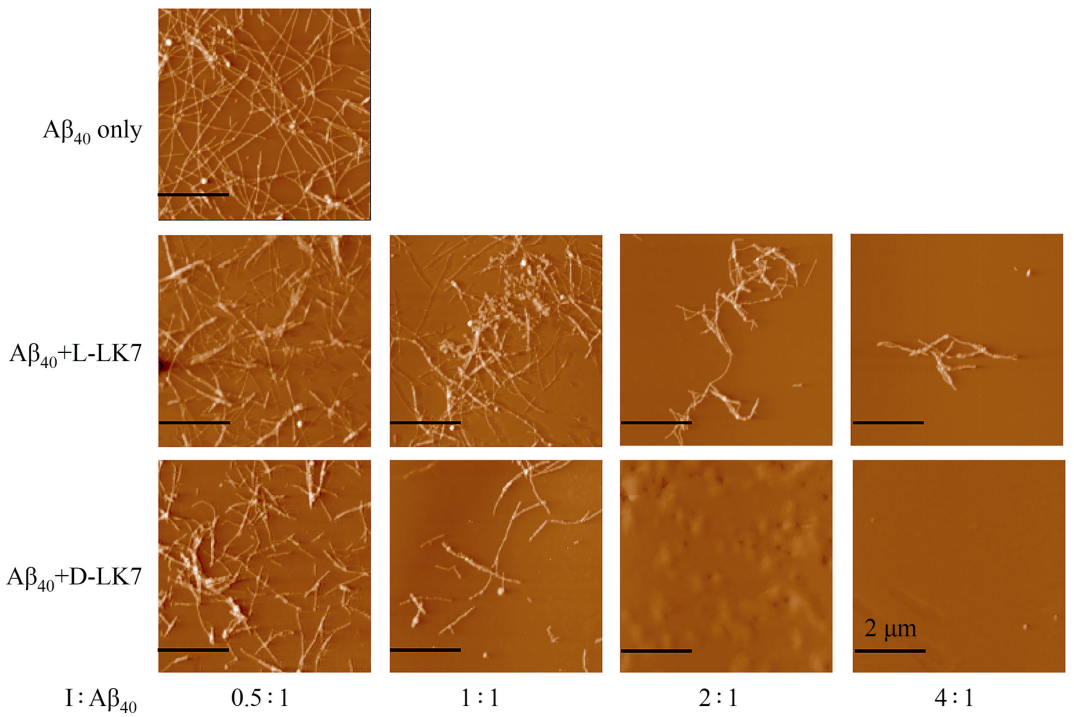

Fig. 4. AFM images of 25 μmol·L^{-1} $A\beta_{40}$ incubated with or without different concentrations of L-LK7 or D-LK7. The molar ratio in the bottom is inhibitor to $A\beta_{40}$.

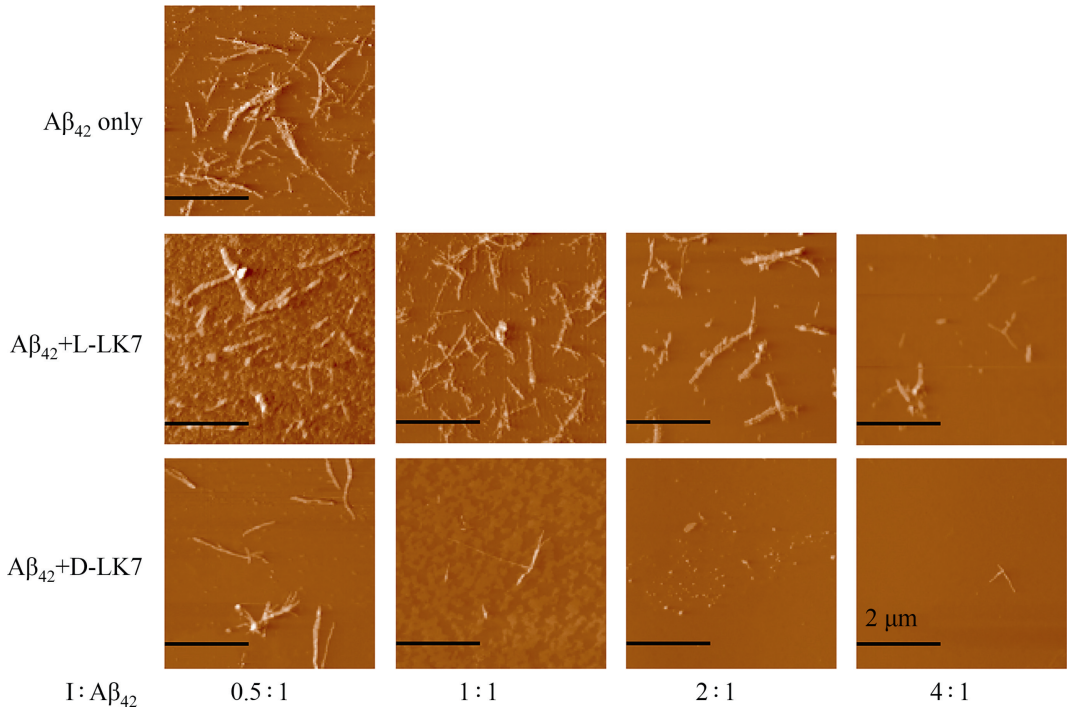

Fig. 5. Influence of the enantiomers on the morphology of 25 μmol·L^{-1} Aβ$_{42}$ aggregates measured by AFM imaging. The ratio in the bottom represents the molar ratio of inhibitor to Aβ$_{42}$.

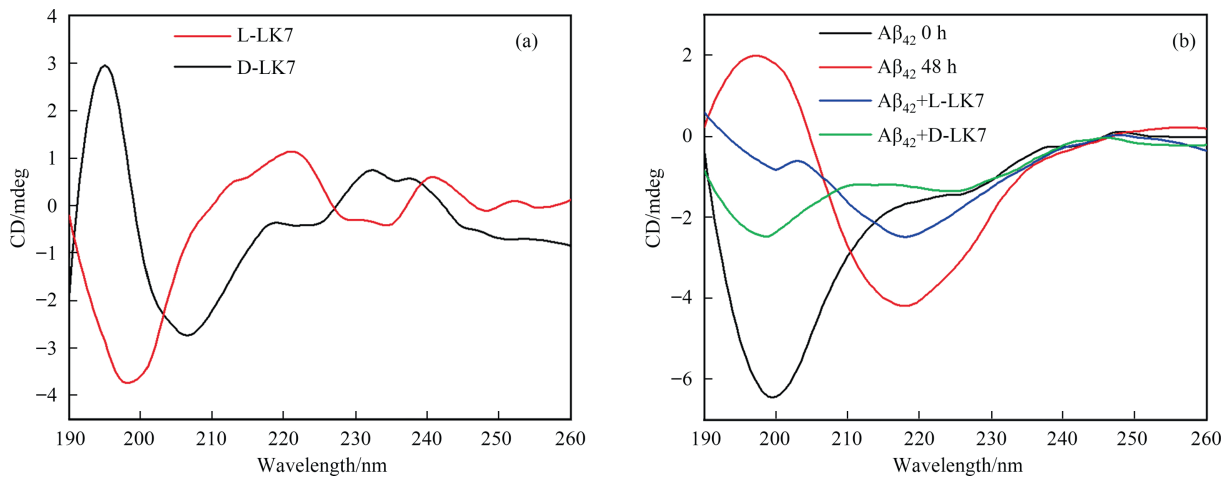

Fig. 6. CD spectra of enantiomers and Aβ$_{42}$ aggregates. (a) The concentration of two enantiomers was 200 μmol·L^{-1}. (b) Aβ$_{42}$ (25 μmol·L^{-1}) at 0 h or incubated with equimolar L-LK7/D-LK7 for 48 h.

the inhibitory efficiency of the enantiomers, secondary structures of Aβ$_{42}$ incubated with equimolar L-LK7/D-LK7 were calculated and are listed in Table 2. The β-sheet content of Aβ$_{42}$ at 48 h decreased from 47.6% to 34.6% with L-LK7, and it reduced to 20.4% with D-LK7. This conforms that D-LK7 was more effective than L-LK7 in inhibiting on-pathway Aβ$_{42}$ conformational transition.

3.4. Enantiomers rescue cytotoxicity and scavenge Aβ plaques in nematodes

The success in suppression of β-sheet structures and fibrillar aggregates formation prompted us to investigate whether enantiomers could decrease Aβ-mediated cytotoxicity and amyloid levels in nematodes. MTT cell viability was performed to test the

Table 2
Secondary structures of Aβ$_{42}$ calculated from 200 – 260 nm spectrum data in Fig. 6 using BeStSeL web server (http://bestsel.elte.hu/)

	Helix/%	β-sheet/%	Turn/%	Others/%
Aβ$_{42}$ (0 h)	4.3	23.8	16.4	55.5
Aβ$_{42}$ (48 h)	2.5	47.6	7.4	42.6
Aβ$_{42}$ + L-LK7 (48 h)	1.5	34.6	12.4	51.5
Aβ$_{42}$ + D-LK7 (48 h)	4.3	20.4	20.3	55

effects of chiral heptapeptides on SH-SY5Y cells. In the absence of $A\beta_{42}$, enantiomers could decrease the cell viability to 87%-74% within the tested concentration range (Fig. 7(a)), indicating slight cytotoxicity. The amyloid-like L-LK7 and D-LK7 fibrils formed by self-assembly could interact with cell membrane and disrupt the membrane functions, leading to the decrease of cell viability. To ameliorate the cytotoxicity caused by enantiomeric LK7 aggregates, one way that can be considered is to conjugate the heptapeptide onto nanoparticles, which would eliminate the self-assemble of enantiomers [21].

However, both L-LK7 and D-LK7 possessed the ability to rescue SH-SY5Y cells from $A\beta_{42}$-induced cytotoxicity. As illustrated in Fig. 7(b), pre-incubated $A\beta_{42}$ species could reduce the cell viability to 60%. L-LK7 alleviated cell viability to 76% at molar ratio of 2:1 (L-LK7:$A\beta_{42}$), but further increase of L-LK7 concentration caused a decline in cell viability, indicating the moderate detoxification of L-LK7. In contrast, D-LK7 rescued cell viability to 68%, 80%, 84% and 83% at the molars ratio of D-LK7:$A\beta_{42}$ at 0.5:1, 1:1, 1:2 and 1:4, respectively, proving its effective detoxification. It is considered that the enantiomers could change the on-pathway aggregation of Aβ, so the formation of neurotoxic Aβ species was significantly suppressed, resulting in the enhanced cell viability. The MTT cell viability test further confirms the superiority of D-LK7 over L-LK7 on alleviating $A\beta_{42}$-mediated cytotoxicity.

For evaluating the *in vivo* inhibitory efficiency of enantiomeric heptapeptides, transgenic *C. elegans* strain CL2006 that expresses human $A\beta_{42}$ peptide in muscle cells was used as an AD model. As illustrated in Fig. 8, amyloid plaques could be labeled by ThT dye, showing green brilliant fluorescence spots. With the treatment of L-LK7/D-LK7, the green spots in nematode were decreased and van-

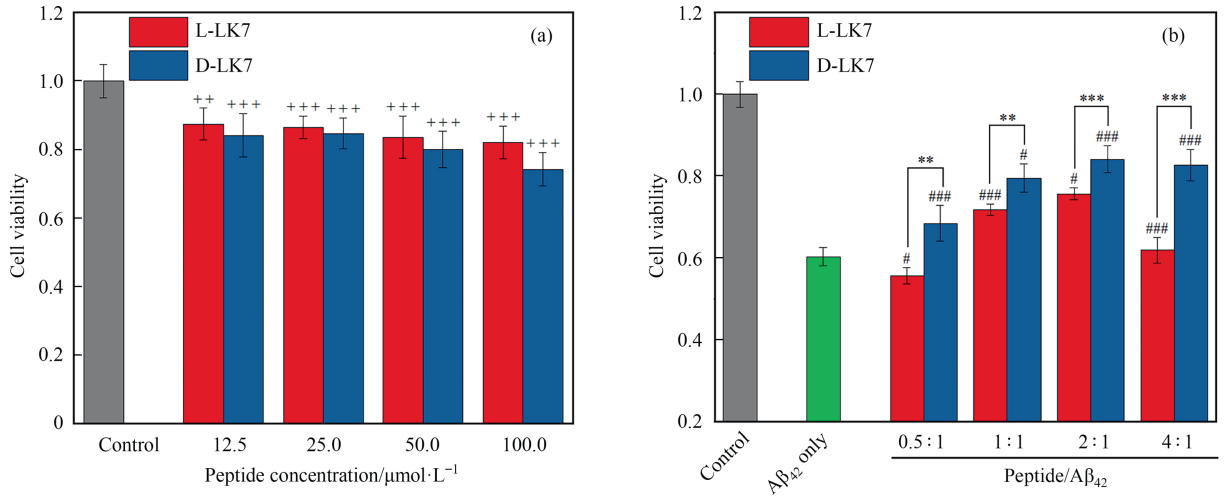

Fig. 7. MTT cell viability assays. (a) The cell viability of SH-SY5Y cells after treating with L-LK7/D-LK7 for 24 h. (b) The detoxification of L-LK7/D-LK7 on $A\beta_{42}$-induced toxicity. The $A\beta_{42}$ concentration was 25 μmol·L^{-1}, which became 5 μmol·L^{-1} in the culture medium due to a 5-fold dilution. Error bars represent standard deviations (n = 6). Statistical significance level is expressed by plus (in comparison with the control group, ++p < 0.01, +++p < 0.001), pound (in comparison with $A\beta_{42}$ only group, #p < 0.05, ###p < 0.001) and asterisk (in comparison with L-LK7 group, **p < 0.01, ***P < 0.001).

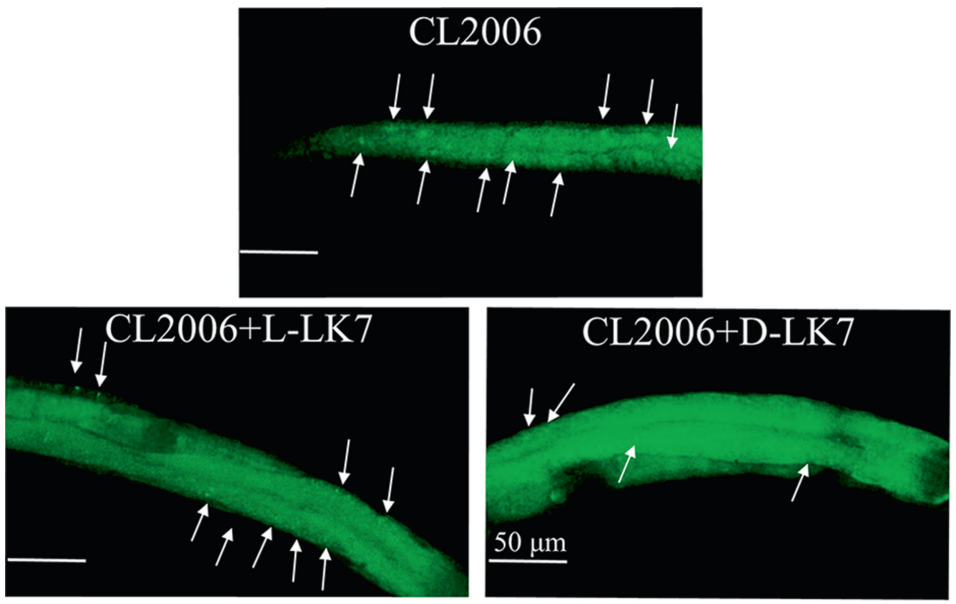

Fig. 8. Fluorescence imaging of Aβ deposits in *C. elegans* (CL2006). The nematodes were treated with L-LK7/D-LK7 for 3 days and then stained with ThT dye.

ished. The nematode treated with D-LK7 showed less Aβ plaques, which is consistent with the *in vitro* results. These results demonstrate that the *in vivo* amyloid deposition could be significantly inhibited by D-LK7.

3.5. Molecular interaction analyses

To understand the molecular mechanisms of chiral heptapeptides with monomeric Aβ, molecular docking was performed using AutoDock Vina. The best conformations are illustrated in Fig. 9 and the corresponding interactions are listed in Table 3. For $A\beta_{40}$ monomer, the binding sits of L-LK7 on $A\beta_{40}$ were identified as a cavity-like domain encompassing the amino acids Tyr10, Val12, Gln15 and Glu22 (Fig. 9(a)), which could further block the hydrophobic interactions during $A\beta_{40}$ aggregation. Besides the above mentioned amino acids, D-LK7 interacted with Gly9 and had higher binding energy of −6.2 kcal·mol^{-1} (1 kcal=4.186 kJ) to $A\beta_{40}$ than −5.8 kcal·mol^{-1} of L-LK7. For $A\beta_{42}$ monomer, L-LK7 was positioned in the N-terminus of $A\beta_{42}$ and interacted with Glu3 and Asp7. However, electrostatic interactions with His6, Asp7, Glu11 and His14 of $A\beta_{42}$ were observed for D-LK7. The favorable conformation provided by D-LK7 led to higher binding energy (−4.4 kcal·mol^{-1}) to $A\beta_{42}$ than L-LK7 (−4.1 kcal·mol^{-1}), causing enhanced inhibitory efficiency on Aβ fibrillization. It is considered that the difference in molecular recognition of enantiomers towards Aβ monomers (Fig. 9) leads to varied performances on suppression of Aβ aggregation (Figs. 1, 2, 4 and 5), conformational transition (Fig. 6), aggregation-related cytotoxicity (Fig. 7) and *in vivo* biological effects (Fig. 8). Thus, the LK7 could inhibit Aβ self-assembly in a chiral-dependent manner.

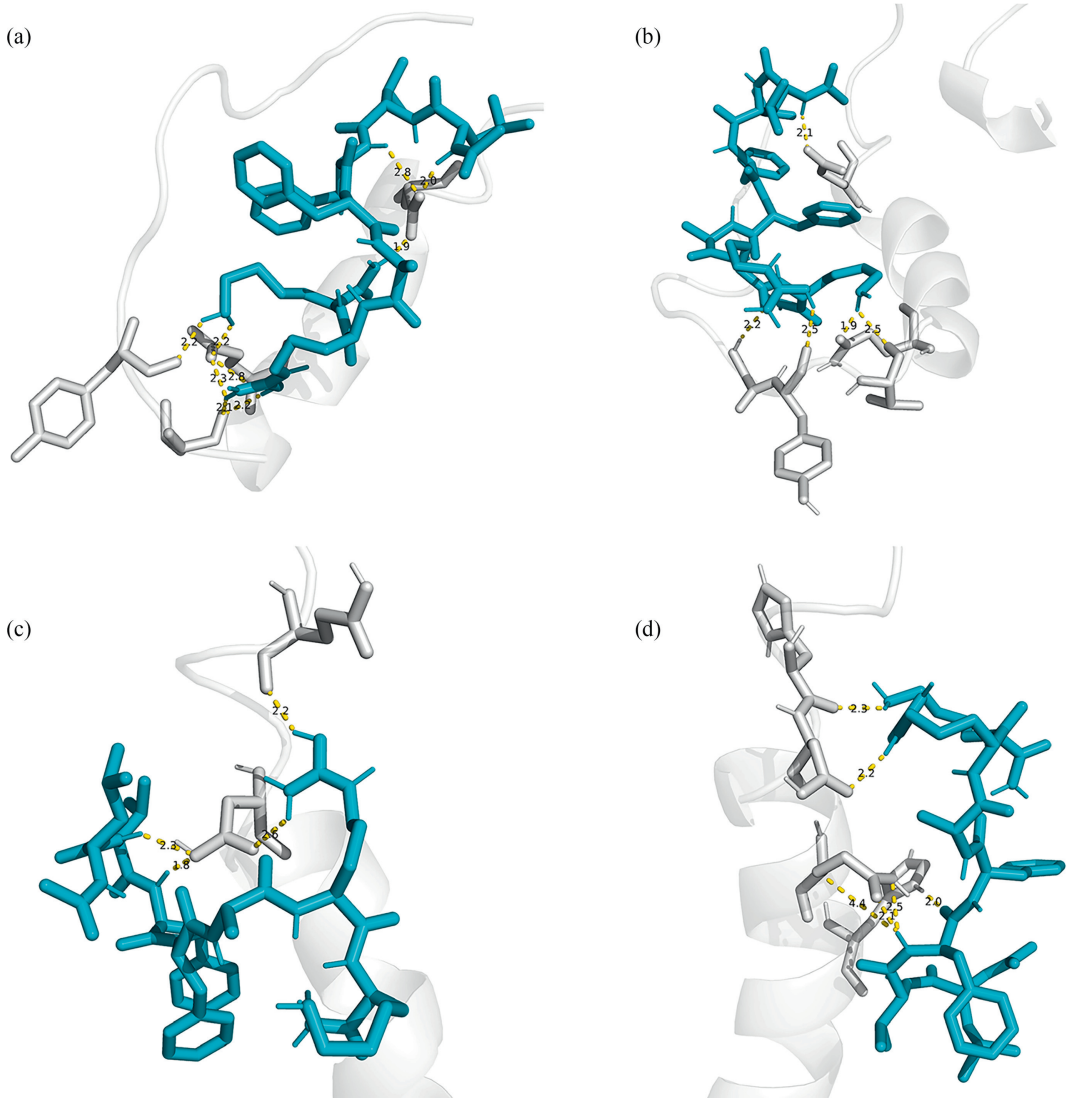

Fig. 9. Docking modes of enantiomeric LK7 with Aβ monomers. (a) L-LK7-$A\beta_{40}$ (PDB ID: 2LFM) complex. (b) D-LK7-$A\beta_{40}$ complex. (c) L-LK7-$A\beta_{42}$ (PDB ID: 1IYT) complex. (d) D-LK7-$A\beta_{42}$ complex.

Table 3
Interactions of enantiomeric LK7 with Aβ monomers summarized from Fig. 9. The EI represents electrostatic interaction

	Model	Interacting amino acid	Mode of interaction	Bond distance/nm	Binding energy/kcal·mol^{-1}
L-LK7	2LFM	Tyr10	H-bond	0.22	−5.8
		Val12	H-bond	0.21	
		Val12	H-bond	0.22	
		Gln15	H-bond	0.22	
		Gln15	H-bond	0.23	
		Gln15	H-bond	0.28	
		Glu22	EI	0.19	
		Glu22	EI	0.20	
		Glu22	EI	0.28	
	1IYT	Glu3	EI	0.22	−4.1
		Asp7	EI	0.18	
		Asp7	EI	0.23	
		Asp7	EI	0.26	
D-LK7	2LFM	Gly9	H-bond	0.22	−6.2
		Tyr10	H-bond	0.25	
		Val12	H-bond	0.25	
		Gln15	H-bond	0.19	
		Glu22	EI	0.21	
	1IYT	His6	EI	0.23	−4.4
		Asp7	EI	0.22	
		Glu11	EI	0.21	
		Glu11	EI	0.25	
		Glu11	EI	0.44	
		His14	EI	0.20	

4. Conclusions

To elucidate the chiral influence of peptide-based inhibitors on Aβ aggregates formation, the effects of heptapeptide L-LK7 was investigated by comparison with D-LK7. Despite the enantiomers could inhibit Aβ fibrillization in a concentration-dependent manner, the D-enantiomer showed enhanced suppression on Aβ aggregation, as evidenced by the lower ThT fluorescence intensity, less visible Aβ aggregates, fewer β-sheet content and better SH-SY5Y cells rescue ability when compared with L-enantiomer under the same conditions. The chiral discrimination of enantiomeric heptapeptides was further formulated by molecular docking calculation, indicating the different inhibition efficiency of enantiomers was due to varied molecular interactions and recognition towards Aβ monomers. This work may open a new avenue for the design of peptide inhibitors against AD by enantioselectivity.

Declaration of Competing Interest

The authors declare that they have no known competing financial interests or personal relationships that could have appeared to influence the work reported in this paper.

Acknowledgements

This work was supported by the National Natural Science Foundation of China (Nos. 21621004 and 21978207) and the Natural Science Foundation of Tianjin from Tianjin Municipal Science and Technology Commission (No. 19JCZDJC36800).

References

[1] F.U. Hartl, Protein misfolding diseases, *Annu. Rev. Biochem.* 86 (1) (2017) 21–26.
[2] N. Levy, S. Eiler, K. Pradeau-Aubreton, B. Maillot, F. Stricher, M. Ruff, Production of unstable proteins through the formation of stable core complexes, *Nat. Commun.* 7 (2016) 10932.
[3] Y. Zhang, Y. Tang, D. Zhang, Y. Liu, J. He, Y. Chang, J. Zheng, Amyloid cross-seeding between Aβ and hIAPP in relation to the pathogenesis of Alzheimer and type 2 diabetes, *Chin. J. Chem. Eng.* 30 (2021) 225–235.
[4] T.P.J. Knowles, M. Vendruscolo, C.M. Dobson, The amyloid state and its association with protein misfolding diseases, *Nat. Rev. Mol. Cell Biol.* 15 (6) (2014) 384–396.
[5] C. Haass, D.J. Selkoe, Soluble protein oligomers in neurodegeneration: Lessons from the Alzheimer's amyloid β-peptide, *Nat. Rev. Mol. Cell Biol.* 8 (2) (2007) 101–112.
[6] C. Patterson, World Alzheimer Report 2018-The State of The Art of Dementia Research: New Frontiers, Alzheime's Disease International (ADI), London, UK, 2018.
[7] T. Mohamed, A. Shakeri, P.P.N. Rao, Amyloid cascade in Alzheimer's disease: Recent advances in medicinal chemistry, *Eur. J. Med. Chem.* 113 (2016) 258–272.
[8] J. Hardy, D.J. Selkoe, The amyloid hypothesis of Alzheimer's disease: Progress and problems on the road to therapeutics, *Science* 297 (5580) (2002) 353–356.
[9] Y. Huang, L. Mucke, Alzheimer mechanisms and therapeutic strategies, *Cell* 148 (6) (2012) 1204–1222.
[10] D. Goyal, S. Shuaib, S. Mann, B. Goyal, Rationally designed peptides and peptidomimetics as inhibitors of amyloid-β (Aβ) aggregation: Potential therapeutics of Alzheimer's disease, *ACS Comb. Sci.* 19 (2) (2017) 55–80.
[11] W. Liu, X. Dong, Y. Liu, Y. Sun, Photoresponsive materials for intensified modulation of Alzheimer's amyloid-β protein aggregation: A review, *Acta Biomater.* 123 (2021) 93–109.
[12] P.C. Ke, E.H. Pilkington, Y.X. Sun, I. Javed, A. Kakinen, G.T. Peng, F. Ding, T.P. Davis, Amyloidosis: Mitigation of amyloidosis with nanomaterials, *Adv. Mater.* 32 (18) (2020) 2070146.
[13] M. Zhang, X. Mao, Y. Yu, C.-X. Wang, Y.-L. Yang, C. Wang, Nanomaterials for reducing amyloid cytotoxicity, *Adv. Mater.* 25 (28) (2013) 3780–3801.
[14] J. Sevigny, P. Chiao, T. Bussière, P.H. Weinreb, L. Williams, M. Maier, R. Dunstan, S. Salloway, T. Chen, Y. Ling, J. O'Gorman, F. Qian, M. Arastu, M. Li, S. Chollate, M.S. Brennan, O. Quintero-Monzon, R.H. Scannevin, H.M. Arnold, T. Engber, K. Rhodes, J. Ferrero, Y. Hang, A. Mikulskis, J. Grimm, C. Hock, R.M. Nitsch, A. Sandrock, The antibody aducanumab reduces Aβ plaques in Alzheimer's disease, *Nature* 537 (7618) (2016) 50–56.
[15] F. Liu, W. Zhao, F. Zhao, Q. Dong, Y. Wang, W. Wei, L. Jia, L.i. Li, F. Lu, Dual effect of the acidic polysaccharose ulvan on the inhibition of amyloid-β protein fibrillation and disintegration of mature fibrils, *ACS Appl. Mater. Interfaces* 12 (37) (2020) 41167–41176.
[16] D.J. Craik, D.P. Fairlie, S. Liras, D. Price, The future of peptide-based drugs, *Chem. Biol. Drug Des.* 81 (1) (2013) 136–147.
[17] S. Bansal, I.K. Maurya, N. Yadav, C.K. Thota, V. Kumar, K. Tikoo, V.S. Chauhan, R. Jain, C-terminal fragment, $Aβ_{32-37}$, analogues protect against Aβ aggregation-induced toxicity, *ACS Chem. Neurosci.* 7 (5) (2016) 615–623.
[18] P.-N. Cheng, C. Liu, M. Zhao, D. Eisenberg, J.S. Nowick, Amyloid β-sheet mimics that antagonize protein aggregation and reduce amyloid toxicity, *Nat. Chem.* 4 (11) (2012) 927–933.
[19] A.N. Klein, T. Ziehm, T. van Groen, I. Kadish, A. Elfgen, M. Tusche, M. Thomaier, K. Reiss, O. Brener, L. Gremer, J. Kutzsche, D. Willbold, Optimization of D-peptides for Aβ monomer binding specificity enhances their potential to eliminate toxic aβ oligomers, *ACS Chem. Neurosci.* 8 (9) (2017) 1889–1900.
[20] J. Liu, W. Wang, Q. Zhang, S. Zhang, Z. Yuan, Study on the efficiency and interaction mechanism of a decapeptide inhibitor of β-amyloid aggregation, *Biomacromolecules* 15 (3) (2014) 931–939.

[21] N. Xiong, X. Dong, J. Zheng, F. Liu, Y. Sun, Design of LVFFARK and LVFFARK-functionalized nanoparticles for inhibiting amyloid β-protein fibrillation and cytotoxicity, *ACS Appl. Mater. Interfaces* 7 (10) (2015) 5650–5662.
[22] H. Zhang, X. Dong, F. Liu, J. Zheng, Y. Sun, Ac-LVFFARK-NH_2 conjugation to β-cyclodextrin exhibits significantly enhanced performance on inhibiting amyloid β-protein fibrillogenesis and cytotoxicity, *Biophys. Chem.* 235 (2018) 40–47.
[23] H. Zhang, C. Zhang, X. Dong, J. Zheng, Y. Sun, Design of nonapeptide LVFFARKHH: A bifunctional agent against Cu^{2+} -mediated amyloid β-protein aggregation and cytotoxicity, *J. Mol. Recognit.* 31 (6) (2018) e2697.
[24] N. Gao, Z. Du, Y. Guan, K. Dong, J. Ren, X. Qu, Chirality-selected chemical modulation of amyloid aggregation, *J. Am. Chem. Soc.* 141 (17) (2019) 6915–6921.
[25] D. Sun, W. Zhang, Q. Yu, X. Chen, M. Xu, Y. Zhou, J. Liu, Chiral penicillamine-modified selenium nanoparticles enantioselectively inhibit metal-induced amyloid β aggregation for treating Alzheimer's disease, *J. Colloid Interface Sci.* 505 (2017) 1001–1010.
[26] W.F. Kean, H.E. Howard-Lock, C.J.L. Lock, Chirality in antirheumatic drugs, *Lancet* 338 (8782-8783) (1991) 1565–1568.
[27] G. Nyström, M. Arcari, R. Mezzenga, Confinement-induced liquid crystalline transitions in amyloid fibril cholesteric tactoids, *Nat. Nanotechnol.* 13 (4) (2018) 330–336.
[28] G.Y. Qing, S.L. Zhao, Y. Xiong, Z. Lv, F.L. Jiang, Y. Liu, H. Chen, M.X. Zhang, T.L. Sun, Chiral effect at protein/graphene interface: A bioinspired perspective to understand amyloid formation, *J. Am. Chem. Soc.* 136 (30) (2014) 10736–10742.
[29] N. Rubin, E. Perugia, M. Goldschmidt, M. Fridkin, L. Addadi, Chirality of amyloid suprastructures, *J. Am. Chem. Soc.* 130 (14) (2008) 4602–4603.
[30] X.B. Zhou, J. Sun, T.T. Yin, F.L. Le, L.C. Yang, Y.N. Liu, J. Liu, Enantiomers of cysteine-modified SeNPs (D/LSeNPs) as inhibitors of metal-induced Aβ aggregation in Alzheimer's disease, *J. Mater. Chem. B* 3 (39) (2015) 7764–7774.
[31] K. Wiesehan, J. Stöhr, L. Nagel-Steger, T. van Groen, D. Riesner, D. Willbold, Inhibition of cytotoxicity and amyloid fibril formation by a D-amino acid peptide that specifically binds to Alzheimer's disease amyloid peptide, *Protein Eng. Des. Sel.* 21 (4) (2008) 241–246.
[32] W. Liu, W. Wang, X. Dong, Y. Sun, Near-infrared light-powered Janus nanomotor significantly facilitates inhibition of amyloid-β fibrillogenesis, *ACS Appl. Mater. Interfaces* 12 (11) (2020) 12618–12628.
[33] O. Trott, A.J. Olson, AutoDock Vina: Improving the speed and accuracy of docking with a new scoring function, efficient optimization, and multithreading, *J. Comput. Chem.* 31 (2) (2010) 455–461.
[34] S. Vivekanandan, J.R. Brender, S.Y. Lee, A. Ramamoorthy, A partially folded structure of amyloid-beta(1–40) in an aqueous environment, *Biochem. Biophys. Res. Commun.* 411 (2) (2011) 312–316.
[35] O. Crescenzi, S. Tomaselli, R. Guerrini, S. Salvadori, A.M. D'Ursi, P.A. Temussi, D. Picone, Solution structure of the Alzheimer amyloid β-peptide (1–42) in an apolar microenvironment. Similarity with a virus fusion domain, *Eur. J. Biochem.* 269 (22) (2002) 5642–5648.
[36] W. Liu, X. Dong, Y. Sun, D-enantiomeric RTHLVFFARK-NH2: A potent multifunctional decapeptide inhibiting Cu^{2+}-mediated amyloid β-protein aggregation and remodeling Cu^{2+}-mediated amyloid β aggregates, *ACS Chem. Neurosci.* 10 (3) (2019) 1390–1401.
[37] K. Hou, J. Zhao, H. Wang, B. Li, K.X. Li, X.H. Shi, K.W. Wan, J. Ai, J. Lv, D.W. Wang, Q.X. Huang, H.Y. Wang, Q. Cao, S.Q. Liu, Z.Y. Tang, Chiral gold nanoparticles enantioselectively rescue memory deficits in a mouse model of Alzheimer's disease, *Nat. Commun.* 11 (1) (2020) 4790.
[38] M. Li, S.E. Howson, K. Dong, N. Gao, J. Ren, P. Scott, X. Qu, Chiral metallohelical complexes enantioselectively target amyloid β for treating Alzheimer's disease, *J. Am. Chem. Soc.* 136 (33) (2014) 11655–11663.
[39] S. Ma, H. Zhang, X. Dong, L. Yu, J. Zheng, Y. Sun, Head-to-tail cyclization of a heptapeptide eliminates its cytotoxicity and significantly increases its inhibition effect on amyloid β-protein fibrillation and cytotoxicity, *Front. Chem. Sci. Eng.* 12 (2) (2018) 283–295.
[40] W. Gao, W. Wang, X. Dong, Y. Sun, Nitrogen-doped carbonized polymer dots: A potent scavenger and detector targeting Alzheimer's β-amyloid plaques, *Small* 16 (43) (2020) 2002804.
[41] Y. Liang, W. Wang, Y. Sun, X. Dong, Insights into the cross-amyloid aggregation of $A\beta_{40}$ and its N-terminal truncated peptide $A\beta_{11\text{-}40}$ affected by epigallocatechin gallate, *Chin. J. Chem. Eng.* 45 (2022) 284–293.